Automated image analysis and hyperspectral imagery with enhanced dark field microscopy applied to biochars produced at different temperatures

Highlights

- Image analysis detected considerable modifications of PR particles after charring
- SEM micrograph showed nonporous surface on PL particles after 550°C pyrolysis
- EFDM image highlighted CD biochar formed by semi-crystalline aggregates
- Emerging imaging techniques are effective for characterizing biochar properties

Automated image analysis and hyperspectral imagery with enhanced dark field microscopy applied to biochars produced at different temperatures

Ilaria Piccoli[a*], Armida Torreggiani[b], Chiara Pituello[a], Annamaria Pisi[c], Francesco Morari[a], Ornella Francioso[c]

[a]Department Agronomy, Food, Natural resources, Animals and Environment, University of Padova, Viale Dell'Università 16, 35020 Legnaro, Italy

[b]Institute of Organic Synthesis and Photoreactivity (ISOF), National Research Council, Via P. Gobetti, 101 40129 Bologna, Italy

[c]Department of Agricultural and Food Sciences, University of Bologna, Viale Fanin 44, 40127 Bologna, Italy

[*]Corresponding author: ilaria.piccoli@unipd.it

Abstract

Biochar from agricultural biomasses and solid wastes represents a win-win solution for a rationale waste management. Its sustainable usage requires identification and standardization of biochar characteristics. The aim of this work was to identify the physical-chemical and spatial characteristics of biochars from pruning residues (PR), poultry litter (PL), and anaerobic cattle digestate (CD) at two pyrolysis temperatures (350°C and 550°C). The biochar characterization was carried out by applying emerging imagining techniques, the 2D automated optical image analysis and hyperspectral enhanced dark-field microscopy (EDFM), and by SEM analysis. As predictable, the feedstocks composition and the pyrolysis temperature strongly influence the physical structures of the biochar samples. PR biochar was mainly characterized by broken and fragmented structure with irregular and rough particle surface, completely different from the original PR wood cell. The EDFM imaging analysis evidenced the thermal degradation of PR vegetal products, composed primarily by hemicellulose, cellulose and lignin. On the contrary, small and regular particles with smoot surface were produced by the PL pyrolysis, especially at 550°C due to minor PL morphological homogeneity in comparison with the other biomasses. Finally, CD charring was characterized by changes in chemical composition, suggested by a lower pixel intensity. In conclusion, the emerging imagining techniques used in this study showed to be very effective in analyzing some properties of biochars then, they can be considered as promising experimental strategies for detecting the feedstocks and pyrolysis temperature of biochar.

40 KEYWORDS. Pyrolysis temperature, pruning residues, poultry litter, anaerobic cattle
41 digestate, discriminant analysis, hyperspectral imagery.
42

1. Introduction

Biochar is a carbon-rich material produced by burning agricultural biomasses (*e.g.*, crop residues, wood biomass, animal litters) and solid wastes with little or no oxygen (*i.e.*, pyrolysis or ‘‘charring’’) (Sohi, 2012). The abundance of these biomasses and their conversion into biochar are surely promising resources to improve waste management and environment (Tan et al., 2015). In fact, a large number of investigations have highlighted how biochar may have a positive impact on mitigating global warming, soil amendment, enhancing crop yield and carbon storage (Khare and Goyal, 2013; Lehmann, 2007; Lehmann and Joseph, 2009; Sohi, 2012; Verheijen et al., 2014; Whitman et al., 2011; Woolf et al., 2010). The carbon sequestration potential of biochar is attributed to its increase in soil stable C fraction (Kuzyakov et al., 2009; Major et al., 2010) and hence long turnover time in soils. However, several studies have provided examples where turnover times in soil are relatively short (<50 years) (Hilscher and Knicker, 2011; Nguyen et al., 2009) and therefore, its longevity is still debated.

The biochar specific features, including porous structure and pore size distribution, large specific surface area, active surface due to oxygen functional groups and presence of minerals, make it as a possible adsorbent of nutrients or pollutant remover from aqueous solutions, similar to activated carbon (Chun et al., 2004; Fu et al., 2012; Li et al., 2008). There is lots of interest in understanding the behavior of biochar and precise information on how the biochar is made from, and produced. All biochars do not have the same properties since their chemical, structural and morphological characteristics depend on the feedstock types, pyrolysis conditions, rate of heating-slow *versus* fast pyrolysis and the duration of charring (Manyà, 2012; Pituello et al., 2015; Zimmerman

and Gao, 2013), of which, the temperature has been found to have a key role on structural characteristics rather than the biomass feedstocks (Chen et al., 2012).

It is generally accepted that biochars are composed by more or less highly conjugated aromatic ring. These structures become more polycondensed with increasing production temperature (Preston and Schmidt, 2006). Depending on temperature, biochar produced at low-temperatures have a greater reactivity in soils possibly due to their higher available nutrients that may contribute to improve soil fertility (Chan et al., 2008; Day et al., 2005) than biochar yield at high temperatures, enriched in material analogous to activated carbon (Ogawa et al., 2006). The latter char is very brittle and prone to abrade into fine fractions that may be incorporated into the soil mineral fraction or may be easily transported in the environment.

Particle size distribution is critical for transport and distribution operations. A median diameter of about 10 μm increases the dustiness of the very light fraction of biochar (Blackwell et al., 2009) affecting the uniformity of spreading and increasing the health risk for operators and particle drift in the environment. However, little is known about the role of particle size in various soil processes such as the transport of adsorbed contaminants (Oleszczuk et al., 2016), the nutrient release, the soil structure aggregation, etc.. A greater contact area and thus a higher particle-to-particle interactions are favoured by a small particle size and platy shape. However, Joseph et al. (2009) postulated that the large inner porosity of a given biochar particle may make particle size a redundant parameter especially for processes associated to water and nutrient availability. Recently, Pituello et al. (2018) have reported contrasting effects also on aggregate stability of different soils amended with biochar. Biochar application increased the soil surface area in clay-poor soil providing additional interparticle

bonding while in clay-rich soil favored repulsive forces between particles with the same charge and consequently, reduced soil particle aggregation.

Therefore, a particle size and shape characterization may improve the understanding of the behaviour of a wide range of pyrolysis yields important for soil amendment purposes.

The measurement of particle size alone is very complicate and may not be enough sensitive to identify the differences between char samples because of heterogeneous nature of feedstock and pyrolysis effect. Particles having very different shapes, but the same area may be identified as identical. No instrument can really measure the particle size distribution independently by the particle shape. Although it is possible to obtain information about particle shape with laser diffraction (Ma et al., 2001), only imaging analysis allows the real characterization of particle size and shape (Bittelli et al., 2019). Imaging analysis technique is an effective technique both for particle size and shape and can provide a real insight into the nature of particles under pyrolysis process. This technology can quantify the size and shape of particles and it has been demonstrated to be able to differentiate the particles (Polakowski et al., 2014). The system works by using imaging every particle and can report particle size and shape data in terms of both volume and number. The images are also screened using a range of morphological filters to remove such things as partially imaged and/or overlapping particles.

There is a need for characterization and analytical tools that can deal with heterogeneous samples with minimum sample preparation. Several different techniques such as Fourier transform infrared (FT-IR) spectroscopy have been applied for evaluating various pyrolysis products (Cantrell et al., 2012; Pituello et al., 2015;

Srinivasan et al., 2015). However, the lack of spatial information makes FT-IR spectroscopy not successful when chemical composition distribution is needed.

Hyperspectral imagining analysis systems combine conventional imaging and spectroscopy for the identification and quantification of chemical constituents, as well as their location or spatial distribution simultaneously. Hyperspectral enhanced dark-field microscopy (EDFM) is a relatively new inspection technology that provides both spectral and spatial information from the product with high spectral resolution through the analysis of scattered light at pixel-by pixel level (Grahn and Geladi, 2007). Samples are imaged by acquiring hundreds of continuous wavelengths or bands, producing extensive spatial and spectral data for each pixel. Hyperspectral EDFM is specifically designed to give quantitative mapping of surfaces and material identification for heterogeneous samples (Badireddy et al., 2012; Torreggiani et al., 2014; Verebes et al., 2013) as biochars. As most of products, biochar needs to be classified in order to conform to a standard related to its usage. Some classification criteria for other pyrolysis products are available, while none for biochar. For example, according to Australian Environmental Protection Authority biosolids can be classified according to contaminant and stabilization grade which, in turn, determine the permitted uses (NSWEPA, 1997). A desired classification would relate biomass and pyrolysis type with agronomic properties but unfortunately data to develop an appropriate biochar classification framework are still lacking (Joseph et al., 2009). Some authors proposed to cluster feedstock properties according to biochar characteristic, as percentage of organic compounds (Demirbaş, 2001), inorganics composition (Nik-Azar et al., 1997), particle size (Zanzi et al., 2002) or moisture content (Moghtaderi, 2006). Another possible biochar classification has been proposed by Joseph et al. (2009) and includes

biochar properties (*e.g.*, ash content, labile C, pH) as a function of pyrolysis conditions. The authors pointed out the need of more studies to fully characterize the range of biochars that may be applied to soil.

The major objective of this work was to test the ability of new and emerging imagining techniques such as 2D optical image and hyperspectral analysis, to provide physical-chemical and spatial properties of biochars generated by the low temperature pyrolysis from different feedstocks such as vineyard pruning residues, anaerobic digestate and litter poultry. The obtained information will provide a wider picture on the potential agronomic and environmental applications of biochar.

2. Material and methods

2.1 Feedstocks and Biochar Production

Feedstocks were collected from plants and experimental farms located in Veneto Region, North-East Italy: (i) anaerobic digestate (CD) from a biogas plant that uses cattle manure mixed with silage maize (30% c.a.), (ii) dry poultry litter (PL) from Italpollina® Italpollina SpA, Verona and (iii) vineyard pruning residues (PR) from the University farm. Feedstocks were dried overnight at 65 °C until the initial moisture (ranging from 40 to 90 %) dropped to less than 7 % (except for dry poultry litter, moisture content 12%) and then ground to a particle size of less than 2 mm. The samples were pyrolyzed in lid-covered porcelain crucibles (Haldenwanger 79MF) in a muffle furnace, preheated at 100 °C, to a highest heating temperature of, 350 and 550 °C with a heating rate between 16 and 19 °C/min and a residence time of 1 hour. The crucibles were then moved with the lids on and left to cool down at room temperature to

prevent any loss in homogeneity due to accidental combustion. All experimental details have been described in previous paper (Pituello et al., 2015).

The produced biochar was weighted and stored in air-tight Falcon vials prior to further analysis.

2.2 Image analysis based on 2D technique

Size distribution and morphology descriptors of biochar particles were determined using an automated particle system, Morphologi G3 (Malvern Instruments Ltd, Malvern, UK). The instrument gave a detailed analysis by automatically capturing images of the sample scanned with microscopic optics.

Biochar samples were dry dispersed on a glass plate by means of an automated dispersion unit. Each sample was scanned using a 5x optics, on a circular scan area of 4.2 cm radius. Diascopic light was set at 80% intensity and focus was manually adjusted before each measurement. To account for 3-dimensionality of particles, a z stacking was used, resulting in an additional layer above focus of 48.9 µm. The size and shape morphological descriptors were calculated by using the Malvern Morphologi G3 software analyzing at least 500.000 particles for each sample. Intensity mean (I) was calculated as the average of the pixel greyscale levels in the particle, for greyscale images I ranges between 0 (black) and 255 (white).Particle dimensions were quantified in terms of volume (μm^3) and diameter (µm).

Particle shapes were quantified in terms of the following parameters:

Circularity (*C*), a measure of how well an object approximates a perfect circle, was calculated as follows:

$$C = \frac{2\pi A}{P^2} \qquad (1)$$

where A is the particle area and P is the particle perimeter. Circularity ranged between 0 and -1, where 1 corresponds to a perfect circle while irregular objects approached 0.

Convexity (C_x) measures the edge roughness of a particle, and is the ratio between the convex hull perimeter (P_c) and the actual perimeter of an object:

$$C_x = \frac{P_c}{P} \qquad (2)$$

Convexity ranges between 0 and 1. An object with a convexity of 1 indicates a smooth shape because the convex hull perimeter equals actual perimeter in this instance.

Elongation index (E_i), a measurement of the overall symmetry/asymmetry of an object is determined as noted below:

$$E_i = 1 - \frac{width}{length} \qquad (3)$$

where width and length are the shortest and longest object axes. Elongation indicates the symmetry (close to 0) or asymmetry (close to 1) of an object in all directions.

2.3 Enhanced dark-field microscopy and hyperspectral imaging

Ground biochar samples (500 µm) were visualized, in air and at room temperature, *via* their light scattering using an enhanced dark-field illumination system (CytoViva, Auburn, AL) attached to an Olympus microscope. The system consisted of a CytoViva 150 dark field condenser in place of the microscope's original condenser, attached *via* a fibre optic light guide to a Solarc 24 W metal halide light source (Welch Allyn, Skaneateles Falls, NY). Improved optical performances are obtained by pre-aligned Koehler and the main feature of Critical illumination. A 100X oil objective with an iris (Olympus UPlanAPO fluorite, N.A. 1.35–0.55) was an integral part of the system. Spectral data within each pixel of the scanned field of view were captured with a

CytoViva spectrophotometer and integrated CCD camera. The visible near-infrared spectrophotometer operates in the range 400-1000 nm. Spectral data were analysed by using the CytoViva Hyperspectral analysis software program (ENVI 4.4 and ITT Visual Information Solutions). Image processing and analysis involved the building of spectral libraries (spectral endmembers). The spectral endmembers were obtained by the selection of a region of interest on the scanned sample. Finally, Spectral Angle Mapper was used to measure the similarity between the image pixels and endmember pixels.

2.4 Scanning electron microscopy (SEM)

Dry samples of feedstocks (and their pyrolysis products at 550 °C) were mounted on aluminium stubs with silver glue and coated with gold-palladium film using an ion sputtering unit Balzer MED 010 (Balzers Union, Ltd, Balzers, Liechtenstein). The samples were observed under a Philips SEM 515 scanning electron microscope (Philips, Eindhoven, The Netherlands) at 7Kv and the pictures taken with a Nikon 5400 Coolpix digital camera (Nikon, Chiyoda-ku, Tokyo, Japan).

2.5 Statistical Analysis

Temperature effect on biochar morphological parameters was compared by applying the non-parametric paired sign test. Bonferroni correction was then adopted to account for multiple comparisons considering significant at $P \leq 0.05/3 = 0.017$.

To assess the ability of morphological parameters to best predict biochar origin, backward stepwise discriminant analysis (DA) was employed. The descriptors for the initial DA were circularity (C), elongation (E_i), convexity (C_x) and intensity (I). Nine pre-defined groups were taken into account as result of the linear combination of three

matrix types × three pyrolysis temperatures. The multiple discriminant functions, the classification criteria, were determined by a measure of Squared Mahalanobis Distances. Classification criteria were based on within-group pooled covariance matrix considering an equal prior probability of the groups. Multivariate F-tests was then applied on pooled within-group variance and covariance matrices in order to determine whether or not there were any significant differences between groups. Canonical correlation analysis was used to extract canonical roots and case scores. Only the roots found statistically significant were used to plot group structure.

Statistical analyses were carried out using Statistica version 10 (Stat Soft. Inc., Tulsa, OK, USA).

3. Results and discussion

3.1 Property of feedstocks and Biochar

Chemical, physical and structural compositions of biochars at different pyrolysis temperatures were described by Pituello et al. (2015). All the feedstocks had a neutral reaction, except CD that was alkaline (pH 8.3). Electrical Conductivity (EC) ranged from 412 to 1642 μs cm^{-1}, respectively in PL and CD. In addition, ash content was extremely variable; it ranged from 2.9 to 5.6 wt % in biomass-based feedstocks (CD and PR). Total carbon was > 40 wt %, while total nitrogen content increased from 1.7 to 4.2 wt % going from CD to PL, and it was sensitively lower for PR. The temperature effect on pH value was evident on all the samples but it was particularly relevant on PL samples, as it varied from 6.9 up to 10.2 with an increase in the pyrolysis temperature. The temperature increase caused a U-shaped response trend in the EC values of both CD and PL samples, whereas in the case of PR gave rise to a decrease in EC values. Ash content increased by increasing the temperature and was higher in the feedstocks with low C content, reaching 32% in PL at 550°C (see Supplementary Material section for further details).

3.2 Image analysis based on 2D technique

Size and shape captured by 2D images (Figure 1), detected considerable modifications for PR biochar particles at both pyrolysis temperatures. Some particles displayed heterogeneity in morphology and in grayscale intensity compared to native PR particles. Especially, agglomerates are prevalent at 550°C (see the top row of Figure 1). Polymerization/condensation reactions taking place during pyrolysis were responsible for different heterogeneous aggregates formation in biochar. Furthermore the increased

alkalinity observed at high temperatures was probably related to polymerization/condensation reactions (Gascó et al., 2005; Liang et al., 2016), release of low molecular weight compounds (*i.e.*, water and acids), high concentration in base cations and carbonates (Fidel et al., 2017).

Conversely, these changes were not so strong for the CD and PL biochar particles. In particular, the color and shape of CD biochars appeared similar to unpyrolized material. Instead PL biochar particles displayed a consistent and regular reduction of particles size at both temperatures. Cantrell et al. (2012) observed PL-derived biochar to exhibit the least aromaticity compared to other matrices which could have caused an higher fragmentation with the pyrolysis temperature. These observations suggest that the variability of biochar response to the temperature depends on the feedstock composition, which can be converted into a wide range of shapes from irregular to spherical.

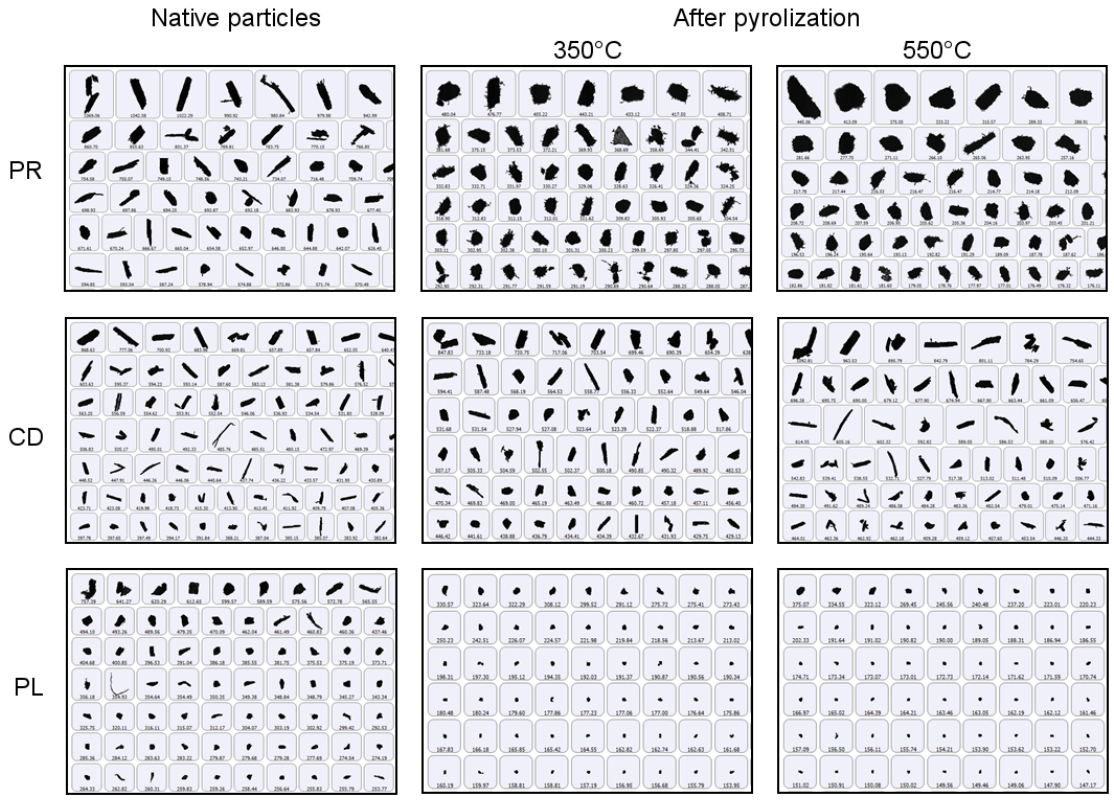

Figure 1. Set of images of different feedstocks, vineyard pruning residues (PR), cattle anaerobic digestate (CD) and poultry litter (PL) before and after pyrolysis at 350°C and 550°C. The biochar particles displayed morphological heterogeneity in PR and CD.

Overall, the shape descriptors as circularity, convexity and elongation are shown in Figure 2.

In PR samples the circularity median values showed statistical difference ($P \leq 0.017$) and in biochars they exhibited smaller values than in their original state (0.504, 0.586 and 0.669 for biochar 350, 550°C and feedstock particles, respectively) A decrease of circularity value suggests that the irregular particles formation was consistent in PR biochar. Similarly, the convexity exhibited a significant ($P \leq 0.017$) decrease in both biochars, 0.807 for 350°C and 0.849°C for 550°C, with respect to PR particles in their original state (0.934). Thus, the PR particles shape of both biochars considerably

292 became irregular and increased the surface roughness as an effect of the temperature.
293 These changes are also supported by a significant (P=0.017) decrease of elongation
294 median values in both biochars, 0.319 and 0.311 for 350°C and 550°C *vs* 0.366 in native
295 particles. The outliers, appearing only after heating, denoted elongation values closer to
296 0 and therefore, they can be classified as "not elongate". This change may be due to the
297 volatilisation process of the external components of the particles, which may lead to a
298 decrease in stability of this outer part of the particles and a subsequent disintegration.

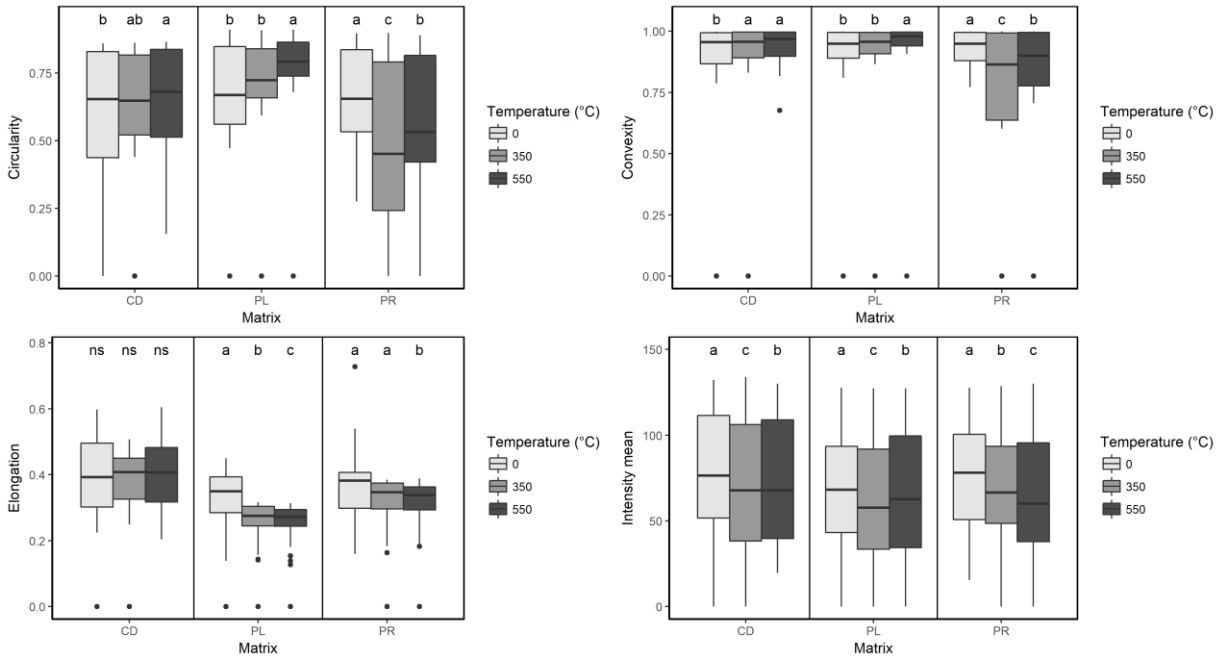

299
300 **Figure 2.** Box plot of vineyard pruning residues (PR), cattle anaerobic digestate (CD)
301 and poultry litter (PL) and biochars at 350° and 550°C descriptors. Different letters
302 indicate statistical differences, according to Bonferroni correction for multiple
303 comparisons conside ($P \leq 0.017$). The box represents the upper (75%) and lower
304 quartile (25%) of the data termed the interquartile range, the horizontal line inside the
305 box is the median of the data, and the ends of the whiskers show the highest and lowest
306 data points.
307

The observed modification was also detectable by SEM micrograph of biochar at 550°C where is clearly visible how the pyrolysis treatment totally modified the wood cell morphological structure originally present, substituting it with a structure completely broken and fragmented (Figure 3a and b). This furthermore supported the reduction in elongation and circularity descriptors.

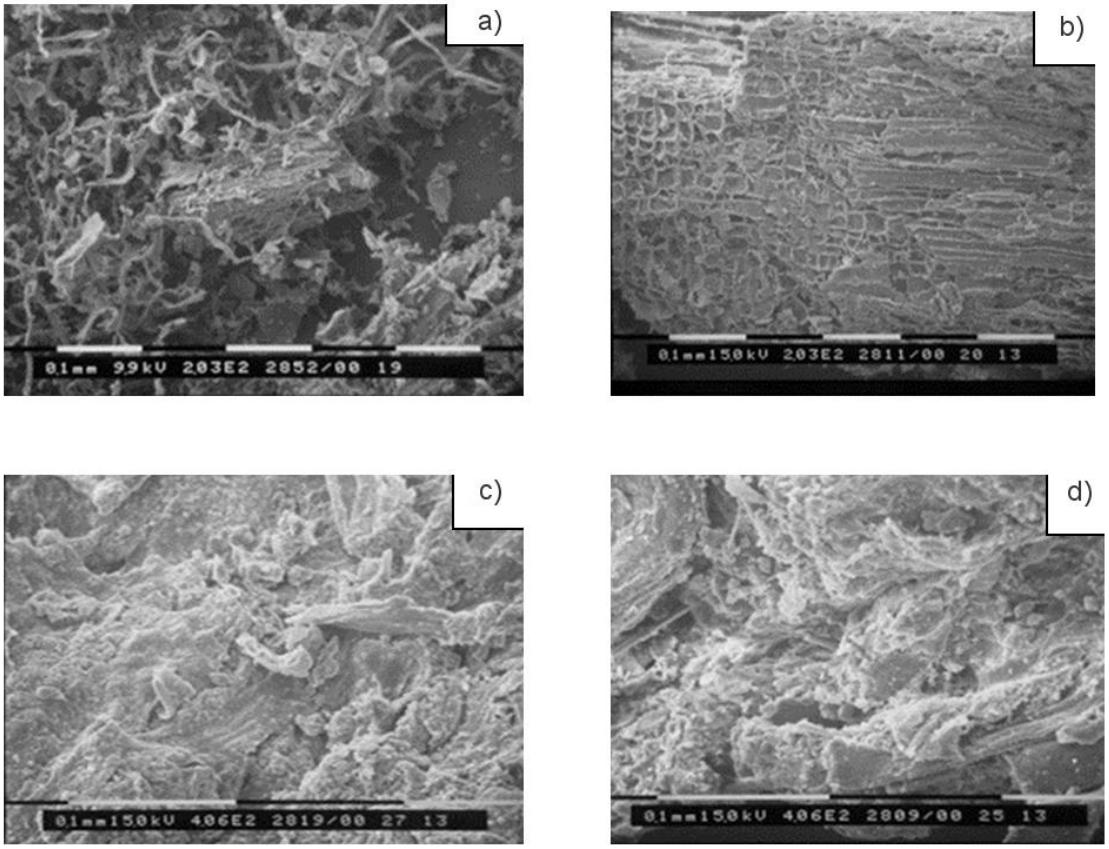

Figure 3. Scanning electron micrographs (SEM) of A) biochar from vineyard pruning residues (PR) yielded at 550 °C; B) unpyrolized PR; C) biochar from poultry litter (PL) yielded at 550°C and D) unpyrolyzed PL.

In PL samples only circularity and convexity median values statistically differed (P = 0.017) in biochar at 550°C (Figure 2). Moreover, both descriptor values were bigger than PL particles in their original state. No statistical difference was found between PL

particles and biochar at 350°C. About elongation median values there were statistical differences (P=0.017) between samples. Especially, elongation values decreased from 0.326 in native particles to 0.261 for 350°C and 0.256 for 550°C biochar, the latter two might be classified as "not elongate". Overall, the pyrolysis temperatures produced smaller particles with regular and smooth surface compared to the poultry litter in original state. This phenomenon was more evident at 550°C.

The SEM micrograph of PL biochar at 550°C (Figure 3c) gave information about the formation of agglomerates with an irregular and nonporous surface.

As regards to CD, no statistical differences were found among the circularity, convexity median and elongation values between biochar obtained at 350°C and 550°C. Conversely, circularity and convexity descriptors increased and statistically (P=0.017) differed from unpyrolized CD particles. Biochar particles at 550°C were mostly regular in size and shape. We can infer that the regularization of biochar particles at 550°C might be as a consequence of enhanced aromaticity and/or occurred minerals calcination (e.g., calcite) as described by Hung et al. 2017).

Pixel intensity showed median values exhibited statistical difference (P = 0.017) in all samples. Their values progressively decreased from 79 in feedstock particles to 72 in both biochars because of the pyrolysis temperature. The variations in pixel intensity could be an indication of differences in composition. Particles containing high-density components may produce higher intensity images. However, because little is known about the application of this technique on biochar, no attempts were made to quantify these differences from the images.

These results suggested that automated particle imaging provided a rapid evaluation between physical descriptors of different feedstocks, pyrolysis temperature and resulting

biochar. These parameters may be considered effective tool for identifying the temperature experienced by feedstock particles at low pyrolysis temperature.

3.3 Hyperspectral analysis

A series of initial measurements were performed in order to evaluate the ability of the Hyperspectral imagery analysis to characterize and differentiate the biochars. All the samples were first imaged *via* light scattering using the EDFM system (as example, Figure 4a) and then the Hyperspectral analysis was performed. Light scattering from PR feedstock gave rise to five spectra **(**Figure 4b**)**. These spectral endmembers were successively used in the image scenes of all samples to perform the spectral mapping. The Spectral Angle Mapper (SAM) classification image showed the distribution of all the five endmembers in the PR image (Figure 4c) and the quantification of their relative abundance (Figure 4d). Bright areas in Figure 4a, corresponding to the black areas in the spectral mapping of Figure 4c, are spectrally unresolved because of their extremely high brightness. Among five spectra, one (Endmember 1) represented the main contribution to the total scattering of PR (~60%). Consequently, it can be considered the most representative for PR feedstock.

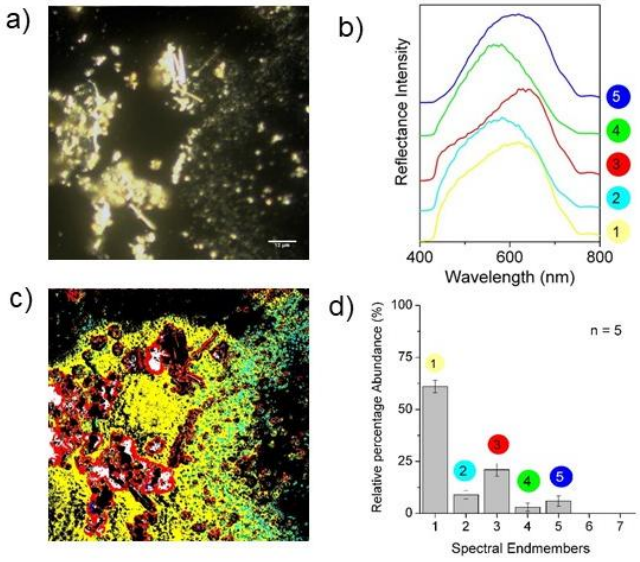

Figure 4. (a) Hyperspectral image (EDFM), (b) Spectral signatures in the 400-800 nm, and (c) Map of the spectral Endmembers in the hyperspectral image of the vineyard pruning residues (PR) obtained by SAM analysis (coloured areas indicate the matching with the spectral profiles); (d) Histogram reporting the relative percentage abundance of the spectral patterns in the maps of hyperspectral images of four PR samples (n standing for the number of the analysed samples). Images were acquired by using 40x objective. All images are 60 μm × 60 μm.

As expected, the pyrolysis at 350 °C induced strong morphological changes in PR biochar, well visible in the EDFM image (Figure 5a). This was also confirmed by the disappearance of the four endmembers contributing to the total scattering of PR feedstock and the presence of two new spectral profiles (Figure 5b). Conversely, little morphological modifications appeared at 550°C (Figure 5d). In fact, the three endmembers mainly contributing to the scattering of the biochar at 350 and 550°C are the same (5, 6, and 7), and only some slight changes in their relative percentage abundance were found (Figure 5b).

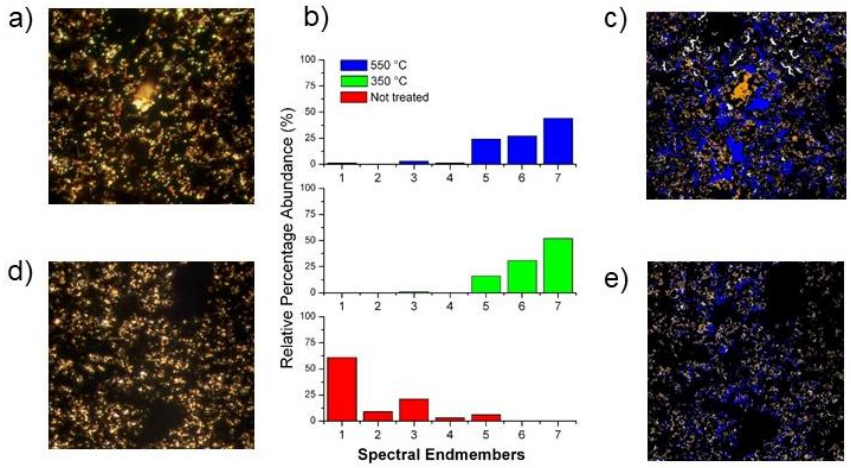

Figure 5. Spectral mapping of vineyard pruning residues (PR) after pyrolysis at 350° and 550°C. (a), (d): EDFM images; (b) Relative percentages abundance of the spectral profiles, revealed by the SAM analysis of the hyperspectral images. For comparison, also the relative percentages obtained before the pyrolysis treatment are reported; (c) and (e): spectral mapping. (a), (c): treated at 350°C; (d), (e): treated at 550°C.

This spectral pattern is characteristic of biochar and can be ascribed to the thermal degradation products of vegetal biomass, composed primarily of hemicellulose, cellulose and lignin. Our results are consistent with thermal analyses under pyrolysis conditions of raw biomass (Rutherford et al., 2012). The major decomposition processes take place from 200 to 500 °C and they are characterized by different steps: i) partial hemicellulose decomposition, (ii) complete hemicellulose decomposition and partial cellulose decomposition, (iii) full cellulose and partial lignin decomposition, and (iv) successive decomposition and increasing degree of carbonization (Rutherford et al., 2012). The disappearance of the Endmember 1, on the basis of descriptor shapes, can be associated to the absence of big particles and the formation of particles classified as "not elongate".

As regards to CD, the further increase in the pyrolysis temperature induced progressive changes in the biochar. In particular, at 550°C bright spots, reflecting light more efficiently, were visible in the EFDM image, indicating the formation of semi-crystalline aggregates, compared with the amorphous structure prevailing in PR biochar (Figure 6). This result is also supported by previous FT-IR spectral profile of biochar from CD which showed a typical band resembling graphite-like carbon or with a low degree of disorder (Pituello et al., 2015). This is based on the relative intensity of the bands at 1437 cm^{-1} (it increases with the number of amorphous carbon structures) and at 1582 cm^{-1}, and it is sharpened as the degree of graphitization increase (Kaufman et al., 1989).

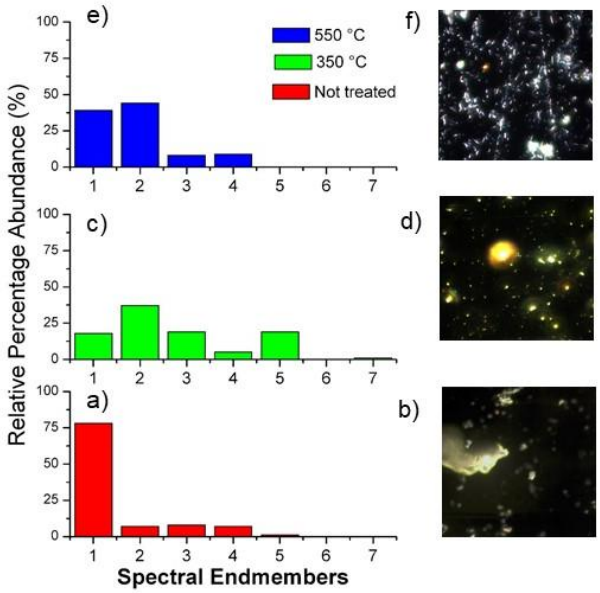

Figure 6. Spectral mapping of cattle anaerobic digestate (CD) samples before and after pyrolysis. (a, c, e) Relative percentages abundance of the spectral profiles, revealed by the SAM analysis of the hyperspectral images, respectively for poultry litter (PL) samples before the heat treatment and after pyrolysis at 350° and 550°C. (b, d, f) EDFM images, respectively for PL samples before and after pyrolysis at the two different temperatures.

The progressive modifications occurring in the CD can be easily followed by hyperspectral analysis: light scattering of the CD feedstock is due to only one Endmember 1, probably for the presence of big and lengthened particles. The latter is still present at the end of the thermal treatment but in a less relevant amount (from ~ 75% to ~ 40%). In addition, the Endmember 2 sensitively increases its contribution, probably because of the formation of anaerobic digestion products in the biochar. Thus, these two spectral profiles (1 and 2) can be considered the most representative for this biochar.

The pyrolysis of PL feedstock induced the strongest changes, clearly visible in the EDFM images of the different spectral patterns at 350 and 550°C (Figure 7). The great susceptibility to the temperature might depend on minor morphological homogeneity of PL in comparison with other feedstocks. As in PR biochar, a significant contribution from the Endmembers 5, 6, 7 was found at 350°C. We can infer that vegetal residues of PL can contribute to this effect. Moreover, PL at 550°C exhibited different spectral patterns in comparison with PR biochar. A spectroscopic characteristic of PL biochar is the progressive increase in the contribution to the total light scattering of the sample from the Endmember 3 (from 3% to 20%, and finally 53%): this behavior can be attributed to the increase of the mineral component (CO_3^{2-}) (Pituello et al., 2015).

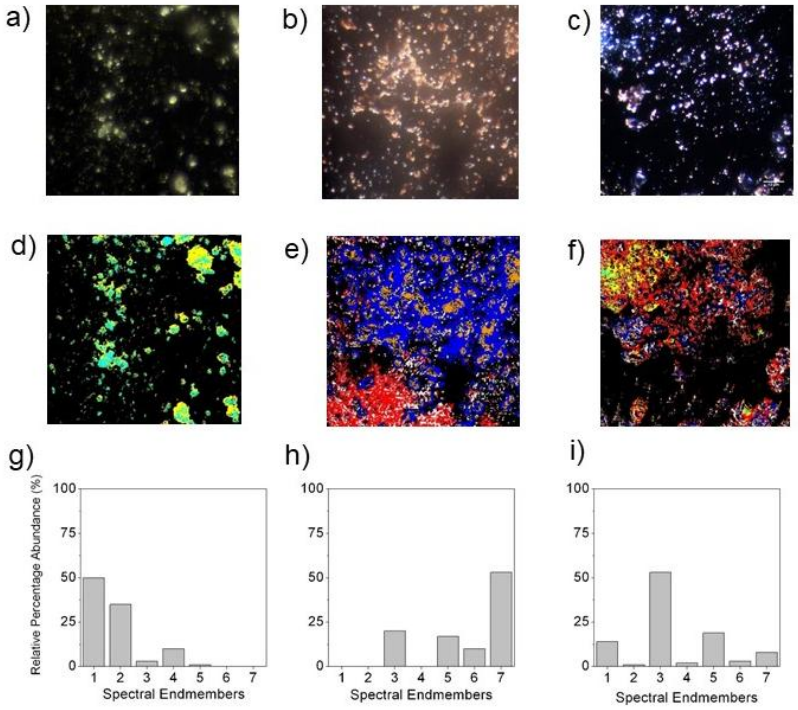

Figure 7. Spectral mapping of poultry litter (PL) samples before and after pyrolysis. (a, b , c): EDFM images of PL samples before the heat treatment and after pyrolysis respectively at 350° and 550°C; (d, e, f) Maps of the spectral Endmembers in the hyperspectral images; (g, h, i) Relative percentages abundance of the spectral profiles, revealed by the SAM analysis of the EDFM images, respectively for PL samples before the heat treatment and after pyrolysis at 350° and 550°C.

3.4 Relationships between image analysis-derived characteristics and different biochar matrices

To determine if the biochar image analysis-derived characteristics can be valid criteria to classify biochar from one another and feedstocks, we carried out the discriminant analysis (DA). The discriminant function was described by circularity, convexity, elongation and intensity mean predictors. Mahalanobis distance among groups pointed out no difference between CD biochars while pyrolysis temperatures significantly

discriminates PR and PL biochars. Four roots were extracted from the matrix and only the first two accounted for 99.9 % ($P< 0.001$) of the total variance of variables. Canonical analysis involved the construction of discriminant functions called "canonical Roots" allowing n-dimensional space objects to be represented on 2D space preserving objects distance order. Root 1 was associated with particle sphericity being positively correlated with circularity and negatively with elongation. Root 2 was representative of particle shape resulting correlated with circularity, convexity and elongation (see Supplementary Material section for further details).

Biochar groups are shown in Figure 8 in the coordinate system of Root 1 (ordinate axis) and 2 (abscissa axis). Root 1 discriminated PL compounds from PR and CD ones being mostly particles characterized by regular circular shape. Root 2 separated PR biochar from its native matrix confirming that pyrolysis strongly affected morphological properties of PR particles. On the contrary CD-derived compounds laid in a clustered area highlighting no differentiation between the CD compounds. Indeed as previously reported, CD particle has been less modified by charring procedure.

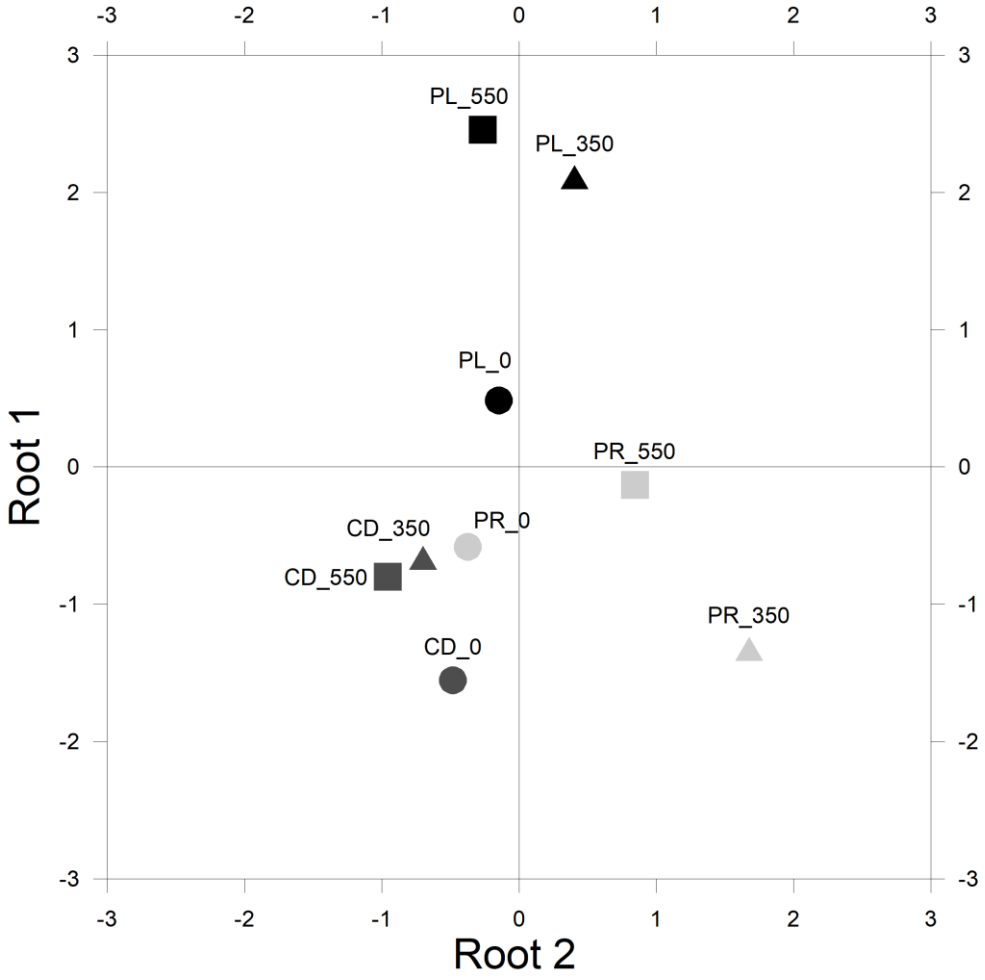

463

464 **Figure 8**. Scatterplot of canonical Root 1 and 2 for the nine pre-defined groups

465 according to the interaction matrix × temperature.

4. Conclusions

The findings show the potentialities of spectral libraries and image analysis to classify biochar according to their feedstocks and the pyrolysis temperature, which strongly influence the physical structures of the biochar samples. In fact, pruning residues and poultry litter-derived biochar underwent the strongest morphological variations after charring, allowing the easiest classification. On the contrary, the analysis of cattle manure digestate, which exhibited smaller changes in its properties after pyrolysis, indicated that other parameters may be helpful for a correct classification of such matrices.

The emerging imagining techniques used in this study showed to be very effective in analyzing some properties of biochars, and they can represent promising experimental strategies for detecting the feedstocks and pyrolysis temperature of biochars. On the other hand, hyperspectral analysis of scattered light, thanks to its property to detect changes in light scattering properties, demonstrated that it is possible to build-up a library of spectral data characteristics of the different morphologies correlated to the chemical composition and heating treatment of the biomasses. On the other hand, image analysis, which is the less expensive technique, showed to be very useful in detecting the original matrix and pyrolysis temperature of biochar, suggesting its potential usage in bio-waste traceability.

Acknowledgments

The authors are extremely grateful to Dr. Carla Marzetti (Antigenia srl Unipersonale), the Italian contact person of Cytoviva company (University of Auburn, AL, USA) for Hyperspectral System Imaging, and to Dr. Carla Ferreri (ISOF-CNR) for providing the CytoViva® hyperspectral microscope. This research did not receive any specific grant from funding agencies in the public, commercial, or not-for-profit sectors.

References

Badireddy, A.R., Wiesner, M.R., Liu, J., 2012. Detection, characterization, and abundance of engineered nanoparticles in complex waters by hyperspectral imagery with enhanced darkfield microscopy. Environ. Sci. Technol. 46, 10081. https://doi.org/10.1021/es204140s

Bittelli, M., Andrenelli, M.C., Simonetti, G., Pellegrini, S., Artioli, G., Piccoli, I., Morari, F., 2019. Shall we abandon sedimentation methods for particle size analysis in soils? Soil Tillage Res. 185, 36–46. https://doi.org/10.1016/J.STILL.2018.08.018

Blackwell, P., Riethmuller, G., Collins, M., 2009. Biochar Application to Soil, in: Lehmann, J., Joseph, S. (Eds.), Biochar for Environmental Management. Earthscan, Gateshead, UK, pp. 207–222.

Cantrell, K.B., Hunt, P.G., Uchimiya, M., Novak, J.M., Ro, K.S., 2012. Impact of pyrolysis temperature and manure source on physicochemical characteristics of biochar. Bioresour. Technol. 107, 419–428. https://doi.org/10.1016/j.biortech.2011.11.084

Chan, K.Y., Van Zwieten, L., Meszaros, I., Downie, A., Joseph, S., 2008. Using poultry litter biochars as soil amendments. Aust. J. Soil Res. 46, 437–444. https://doi.org/10.1071/SR08036

Chen, Z., Chen, B., Zhou, D., Chen, W., 2012. Bisolute sorption and thermodynamic behavior of organic pollutants to biomass-derived biochars at two pyrolytic temperatures. Environ. Sci. Technol. 46, 12476–12483.

514 https://doi.org/10.1021/es303351e

515 Chun, Y., Sheng, G., Chiou, G.T., Xing, B., 2004. Compositions and sorptive properties
516 of crop residue-derived chars. Environ. Sci. Technol. 38, 4649–4655.
517 https://doi.org/10.1021/es035034w

518 Day, D., Evans, R., Lee, J., Reicosky, D., 2005. Economical CO, SO, and NO capture
519 from fossil-fuel utilization with combined renewable hydrogen production and
520 large-scale carbon sequestration. Energy 30, 2558–2579.
521 https://doi.org/10.1016/j.energy.2004.07.016

522 Demirbaş, A., 2001. Carbonization ranking of selected biomass for charcoal, liquid and
523 gaseous products. Energy Convers. Manag. 42, 1229–1238.
524 https://doi.org/10.1016/S0196-8904(00)00110-2

525 Fidel, R.B., Laird, D.A., Thompson, M.L., Lawrinenko, M., 2017. Characterization and
526 quantification of biochar alkalinity. Chemosphere.
527 https://doi.org/10.1016/j.chemosphere.2016.09.151

528 Fu, P., Hu, S., Xiang, J., Sun, L., Su, S., Wang, J., 2012. Evaluation of the porous
529 structure development of chars from pyrolysis of rice straw: effects of pyrolysis
530 temperature and heating rate. J. Anal. Appl. Pyrolysis 98, 177–183.
531 https://doi.org/10.1016/j.jaap.2012.08.005

532 Gascó, G., Blanco, C.G., Guerrero, F., Lázaro, A.M.M., 2005. The influence of organic
533 matter on sewage sludge pyrolysis. J. Anal. Appl. Pyrolysis 74, 413–420.
534 https://doi.org/10.1016/j.jaap.2004.08.007

Grahn, H.F., Geladi, P., 2007. Techniques and Applications of Hyperspectral Image Analysis, Techniques and Applications of Hyperspectral Image Analysis. John Wiley & Sons, Ltd, Chichester, West Sussex. https://doi.org/10.1002/9780470010884

Hilscher, A., Knicker, H., 2011. Carbon and nitrogen degradation on molecular scale of grass-derived pyrogenic organic material during 28 months of incubation in soil. Soil Biol. Biochem. 43, 261–270. https://doi.org/10.1016/j.soilbio.2010.10.007

Hung, C.Y., Tsai, W.T., Chen, J.W., Lin, Y.Q., Chang, Y.M., 2017. Characterization of biochar prepared from biogas digestate. Waste Manag. 66, 53–60. https://doi.org/10.1016/j.wasman.2017.04.034

Joseph, S., Peacocke, C., Lehmann, J., Munroe, P., 2009. Developing a biochar classification and test methods, in: Lehmann, J., Joseph, S. (Eds.), Biochar for Environmental Management. Earthscan Ltd, London.

Kaufman, J.H., Metin, S., Saperstein, D.D., 1989. Symmetry breaking in nitrogen-doped amorphous carbon: Infrared observation of the Raman-active G and D bands. Phys. Rev. B. https://doi.org/10.1103/PhysRevB.39.13053

Khare, P., Goyal, D.K., 2013. Effect of high and low rank char on soil quality and carbon sequestration. Ecol. Eng. 52, 161–166. https://doi.org/10.1016/j.ecoleng.2012.12.101

Kuzyakov, Y., Subbotina, I., Chen, H., Bogomolova, I., Xu, X., 2009. Black carbon decomposition and incorporation into soil microbial biomass estimated by 14C labeling. Soil Biol. Biochem. 41, 210–219.

https://doi.org/10.1016/j.soilbio.2008.10.016

Lehmann, J., 2007. Bio-energy in the black. Front. Ecol. Environ. https://doi.org/10.1890/1540-9295(2007)5[381:BITB]2.0.CO;2

Lehmann, J., Joseph, S., 2009. Biochar for environmental management: science and technology, Science And Technology.

Li, W., Yang, K., Peng, J., Zhang, L., Guo, S., Xia, H., 2008. Effects of carbonization temperatures on characteristics of porosity in coconut shell chars and activated carbons derived from carbonized coconut shell chars. Ind. Crops Prod. 28, 190–198. https://doi.org/10.1016/j.indcrop.2008.02.012

Liang, C., Gascó, G., Fu, S., Méndez, A., Paz-Ferreiro, J., 2016. Biochar from pruning residues as a soil amendment: Effects of pyrolysis temperature and particle size. Soil Tillage Res. 164, 3–10. https://doi.org/10.1016/j.still.2015.10.002

Ma, Z., Merkus, H.G., Scarlett, B., 2001. Extending laser diffraction for particle shape characterization: Technical aspects and application. Powder Technol. 118, 180–187. https://doi.org/10.1016/S0032-5910(01)00309-6

Major, J., Lehmann, J., Rondon, M., Goodale, C., 2010. Fate of soil-applied black carbon: Downward migration, leaching and soil respiration. Glob. Chang. Biol. 16, 1366–1379. https://doi.org/10.1111/j.1365-2486.2009.02044.x

Manyà, J.J., 2012. Pyrolysis for biochar purposes: A review to establish current knowledge gaps and research needs. Environ. Sci. Technol. https://doi.org/10.1021/es301029g

578 Moghtaderi, B., 2006. The state-of-the-art in pyrolysis modelling of lignocellulosic
579 solid fuels. Fire Mater. 30, 1–34. https://doi.org/10.1002/fam.891

580 Nguyen, B.T., Lehmann, J., Kinyangi, J., Smernik, R., Riha, S.J., Engelhard, M.H.,
581 2009. Long-term black carbon dynamics in cultivated soil, in: Biogeochemistry.
582 pp. 163–176. https://doi.org/10.1007/s10533-008-9248-x

583 Nik-Azar, M., Hajaligol, M.R., Sohrabi, M., Dabir, B., 1997. Mineral matter effects in
584 rapid pyrolysis of beech wood. Fuel Process. Technol. 51, 7–17.
585 https://doi.org/10.1016/S0378-3820(96)01074-0

586 NSWEPA, 1997. Environmental guidelines: use and disposal of biosolids products.
587 Environment Protection Authority, Chatswood, NSW, Australia.

588 Ogawa, M., Okimori, Y., Takahashi, F., 2006. Carbon sequestration by carbonization of
589 biomass and forestation: Three case studies, in: Mitigation and Adaptation
590 Strategies for Global Change. pp. 429–444. https://doi.org/10.1007/s11027-005-
591 9007-4

592 Oleszczuk, P., Ćwikła-Bundyra, W., Bogusz, A., Skwarek, E., Ok, Y.S., 2016.
593 Characterization of nanoparticles of biochars from different biomass. J. Anal.
594 Appl. Pyrolysis 121, 165–172. https://doi.org/10.1016/J.JAAP.2016.07.017

595 Pituello, C., Dal Ferro, N., Francioso, O., Simonetti, G., Berti, A., Piccoli, I., Pisi, A.,
596 Morari, F., 2018. Effects of biochar on the dynamics of aggregate stability in clay
597 and sandy loam soils. Eur. J. Soil Sci. 69, 827–842.
598 https://doi.org/10.1111/ejss.12676

599 Pituello, C., Francioso, O., Simonetti, G., Pisi, A., Torreggiani, A., Berti, A., Morari, F.,
600 2015. Characterization of chemical–physical, structural and morphological
601 properties of biochars from biowastes produced at different temperatures. J. Soils
602 Sediments 15, 792–804. https://doi.org/10.1007/s11368-014-0964-7

603 Polakowski, C., Sochan, A., Bieganowski, A., Ryzak, M., Földényi, R., Tóth, J., 2014.
604 Influence of the sand particle shape on particle size distribution measured by laser
605 diffraction method. Int. Agrophysics 28, 195–200. https://doi.org/10.2478/intag-
606 20014-0008

607 Preston, C.M., Schmidt, M.W.I., 2006. Black (pyrogenic) carbon: A synthesis of current
608 knowledge and uncertainties with special consideration of boreal regions.
609 Biogeosciences 3, 397–420. https://doi.org/10.5194/bg-3-397-2006

610 Rutherford, D.W., Wershaw, R.L., Rostad, C.E., Kelly, C.N., 2012. Effect of formation
611 conditions on biochars: Compositional and structural properties of cellulose, lignin,
612 and pine biochars. Biomass and Bioenergy 46, 693–701.
613 https://doi.org/10.1016/j.biombioe.2012.06.026

614 Sohi, S.P., 2012. Carbon storage with benefits. Science (80-.).
615 https://doi.org/10.1126/science.1225987

616 Srinivasan, P., Sarmah, A.K., Smernik, R., Das, O., Farid, M., Gao, W., 2015. A
617 feasibility study of agricultural and sewage biomass as biochar, bioenergy and
618 biocomposite feedstock: Production, characterization and potential applications.
619 Sci. Total Environ. 512–513, 495–505.
620 https://doi.org/10.1016/j.scitotenv.2015.01.068

621 Tan, X., Liu, Y., Zeng, G., Wang, X., Hu, X., Gu, Y., Yang, Z., 2015. Application of
622 biochar for the removal of pollutants from aqueous solutions. Chemosphere.
623 https://doi.org/10.1016/j.chemosphere.2014.12.058

624 Torreggiani, A., Tinti, F., Savoini, A., Melchiorre, M., Po, R., Camaioni, N., 2014.
625 Hyperspectral imaging of polymer/fullerene blends. Org. Photonics Photovoltaics
626 2. https://doi.org/10.2478/oph-2014-0003

627 Verebes, G.S., Melchiorre, M., Garcia-Leis, A., Ferreri, C., Marzetti, C., Torreggiani,
628 A., 2013. Hyperspectral enhanced dark field microscopy for imaging blood cells. J.
629 Biophotonics. https://doi.org/10.1002/jbio.201300067

630 Verheijen, F.G.A., Graber, E.R., Ameloot, N., Bastos, A.C., Sohi, S., Knicker, H., 2014.
631 Biochars in soils: New insights and emerging research needs. Eur. J. Soil Sci. 65,
632 22–27. https://doi.org/10.1111/ejss.12127

633 Whitman, T., Nicholson, C.F., Torres, D., Lehmann, J., 2011. Climate change impact of
634 biochar cook stoves in western kenyan farm households: System dynamics model
635 analysis. Environ. Sci. Technol. 45, 3687–3694. https://doi.org/10.1021/es103301k

636 Woolf, D., Amonette, J.E., Street-Perrott, F.A., Lehmann, J., Joseph, S., 2010.
637 Sustainable biochar to mitigate global climate change. Nat. Commun. 1.
638 https://doi.org/10.1038/ncomms1053

639 Zanzi, R., Sjöström, K., Björnbom, E., 2002. Rapid pyrolysis of agricultural residues at
640 high temperature. Biomass and Bioenergy 23, 357–366.
641 https://doi.org/10.1016/S0961-9534(02)00061-2

642 Zimmerman, A.R., Gao, B., 2013. The stability of biochar in the environment, biochar
643 and soil biota. CRC Press, Boca Raton, FL.

644